Optimization-Based Strategies for Optimal Inverse Parameters Estimation for Heat Transfer Systems

DAVID MATAJIRA-RUEDA [1], **JORGE MARIO CRUZ-DUARTE** [2], **(Member, IEEE),**
JUAN GABRIEL AVINA-CERVANTES [1],
MARIO ALBERTO IBARRA-MANZANO [1], **(Member, IEEE), AND RODRIGO CORREA** [3]

[1]Engineering Division of Campus Irapuato-Salamanca, Telematics Research Group (CA), Department of Electronics Engineering, University of Guanajuato, Guanajuato 36885, Mexico
[2]Escuela de Ingeniería y Ciencias, Tecnológico de Monterrey, Monterrey 64849, Mexico
[3]Facultad de Ingenierías Físico-Mecánicas, Escuela de Ingenierías Eléctrica, Electrónica y de Telecomunicaciones, Universidad Industrial de Santander, Bucaramanga 680002, Colombia

Corresponding author: Juan Gabriel Avina-Cervantes (avina@ugto.mx)

ABSTRACT Thermal design for electronic devices approached through the solution analysis of the Inverse Heat Transfer Problem (IHTP) has not been extensively explored. This article proposes an alternative strategy and a contrasting approach for the optimal inverse parameters' estimation of heat transfer systems, particularly in designing heat sinks. A framework to tackle a Rectangular Microchannel Heat Sink (RMCHS) design modeled by the Entropy Generation Minimization (EGM) criterion is developed. This framework comprises two strategies to be compared. The serial proposal works sequentially depending on the parameters' sensitivity into the RMCHS model, backpropagating estimated parameters to all processes. The parallel strategy processes all parameters simultaneously. Instead of focusing efforts on a typical optimization process, a sequential procedure takes advantage of the most influential parameters in the heat sink model and the excellent exploration-exploitation rate of Metaheuristic Optimization Algorithms (MOAs). The most sensitive design variables are prioritized in the serial strategy. The implemented estimation-optimization strategies are addressed through an IHTP's inverse analysis. Thereby, global MOAs are implemented to solve the specific application and become an alternative to the gradient-based methods when their efficiency and effectiveness are at stake. MOAs show overall relative errors related to minimal entropy generation rate inferior to 0.07% for data with 30 dB of SNR and less than 7.63% of error for data with 10 dB of SNR compared with the Levenberg-Marquardt method. Numerical results show that serial strategy provided a stable and reliable design solution even with contaminated data, obtaining better performances than the multiparametric strategy. Additionally, parametric and nonparametric statistical tests were used to validate the appropriate optimization algorithm and the most reliable strategy. The statistical tests confirmed the optimal-inverse problem estimation and optimization improvement by combining the serial strategy and analyzed MOAs to design the RMCHS based on the EGM criterion.

INDEX TERMS Inverse heat transfer problem, Levenberg-Marquardt, metaheuristics, optimization algorithms, Rectangular Microchannel Heat Sink.

I. INTRODUCTION

The optimal thermal management for electronic devices is still a relevant topic for the scientific and engineering

The associate editor coordinating the review of this manuscript and approving it for publication was Shunfeng Cheng.

communities since Integrated Circuits appeared and their scale of integration regularly increases [1]. In this context, the Rectangular Microchannel Heat Sink (RMCHS) proposed by Tuckerman and Pease [2] is a common and suitable solution to address this problem when high power dissipation is involved [3]–[7]. Sometimes the selection of this mechanical

component is made arbitrarily by practitioners; other times, the RMCHS is designed for a particular device. In any case, a complimentary design stage is included for revising and refining the overall implementation, but it is mostly limited to the system thermal behavior. So, there is not guarantee that the optimal performance, according to the Second Law of thermodynamics, is achieved. Recall that, in simple terms, this law indicates how far our system is from its ideal behavior. In scientific literature about thermal design techniques, alternatives exist based on well-known and essential stages such as modeling, simulation, components selecting, and optimization processes. However, the thermodynamic design addressed through inverse analysis has not been widely explored.

On the one hand, IHTP inverse analysis is a powerful tool when classical property estimation techniques are unsuitable or inaccurate to cope with ill-conditioned models [3]–[5], [8]. When solving an IHTP, the Direct Problem (DP) solution determines the effects derived directly from the external causes. For instance, this could find temperature profiles from the thermal model, including the heat transfer conduction, convection, and radiation mechanisms. However, in the Inverse Problem (IP) solution, the major causes are estimated from information related to known effects under particular conditions and using the related physical foundations [9], [10]. Formally, the inverse analysis obeys the Hadamard conditions, where a solution must exist, be unique, and stable to minor disturbances [9]. Here, the problem is considered ill-posed if the solution can become unstable due to accumulated errors, disturbances, or noisy input data. Thereby, regularization techniques use IP as a DP reformulation to lead convergence and stabilizing results [11]–[13]. Especially in the IHTP solution, temperature measurements are used to estimate the intrinsic system features, such as heated body geometric characteristics, thermal sources, initial conditions, thermophysical properties, and boundary conditions [10]. In such regard, IHTP inverse analysis and fully-developed numerical tools can improve thermal-management performance in microchannel heat sinks design, refining the geometry profile, even its building material, and working fluid for specific purposes [14]–[16].

On the other hand, the current literature reveals that the most common and discriminant variables concerning the designing of RMCHS are the number of channels, channel aspect ratio, and width ratio of the channel to pitch [3]–[5]. Notwithstanding, recent publications have considered other characteristics such as the effects, nature, and physical properties of the heat sink body material and cooling fluids [4], [17], [18]. Theoretically, classical approaches for designing heat sinks are generally based on the thermodynamics second law [19]. Recently, Khan *et al.* [20] proposed a design model based on the Entropy Generation Minimization (EGM) criterion from the Second Law of thermodynamics. It quantifies the thermodynamic irreversibilities of the active working system due to heat transfer and fluid flow processes [7], [21]. Furthermore, there is an exponentially

increasing trend of new proposals and applications solved by MOAs [9], [22]–[24].

In this study, the inverse analysis includes five phases supported by the MOAs: DP and IP descriptions, iterative procedure, stopping criteria, and computational algorithm. MOAs aim to obtain similar and precise results sans requiring analytical derivatives and a close-convergent starting point. These characteristics are highly needed to implement the Levenberg-Marquardt (LM) algorithm. Indeed, there were implemented five MOAs as alternatives to LM for minimizing the Ordinary Least Squares Norm as the cost function in the inverse analysis. These are metaheuristics that include the Electromagnetic Field Optimization (EFO) [25], Unified Particle Swarm Optimization (UPSO) [26], Differential Evolution (DE) [27], Spiral Optimization (SO) [28], and Simulated Annealing (SA) [29]. Such algorithms were chosen because they are well-known for their relative simplicity for programming using a reduced number of tuning parameters, a fast converging rate, and an excellent balance between exploitation and exploration behaviors. In addition, two different strategies (serial and parallel) to implement the MOAs and address the IHTP were considered for this study. As a practical problem, the inverse analysis was selected to find the optimal design parameters (say, those related to geometry, building material, and working fluid) on the RMCHS modeled by the EGM criterion. To do so, the experimental data were simulated from the temperature profile measurements (multiple sensors at regular intervals) with different noise levels. Plus, the results were compared from the MOA-based implementations against those from LM using the parametric (based on mean and standard deviations) and nonparametric (Wilcoxon-Mann-Whitney, Friedman, and Kruskal-Wallis) tests. Withal, it was proven that metaheuristic algorithms improve the IHTP inverse analysis focused on optimally designing the RMCHS, involving the processing of complex and intricate nonlinear IP and DP. Extensive experimentation was developed to verify the reliability and stability of the overall proposed method, as it is discussed below.

II. MATERIALS AND METHODS
A. RECTANGULAR MICROCHANNEL HEAT SINK
Fig. 1 shows the outline of the analyzed system, including the RMCHS (Part I), the input and output for the fluid flow (Parts II and III), and the thermal interface (Part IV) coupling the electronic device (Part V). RMCHS dimensions are defined as $H_D \times L_D \times W_D$, where $H_D = h_c + t_u + t_l$, h_c [m] is the channel height, t_u [m], and t_l [m] are the upper and lower thicknesses of the parallel plates enclosing the fins array.

1) CONTROL VOLUME DIMENSIONS OF THE RMCHS
Fig. 2 shows the rectangular microchannel dimensions defined by $2w_c \times h_c \times L_D$, with the same length as RMCHS. Furthermore, the wall plate width is defined by $2w_p$, and the number of microchannels N_c is obtained as

$$N_c = \frac{W_D/2 - w_p}{w_c + w_p}, \tag{1}$$
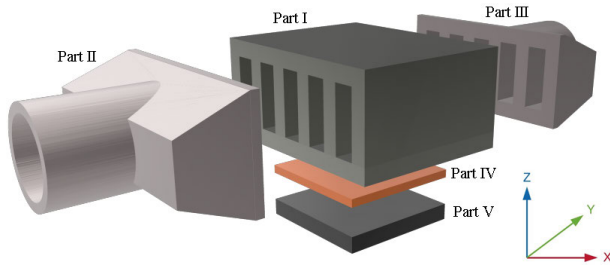
FIGURE 1. Outline of the rectangular micro-channel heat sink system. The component dimensions are over-scaled for illustrative purposes. Part I: heat sink; Parts II and III: input and output for the fluid flow; Part IV: thermal interface; and Part V: electronic device.
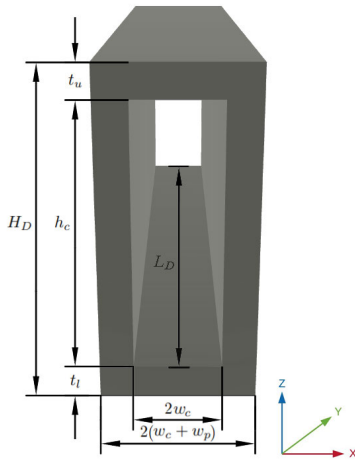
FIGURE 2. Microchannel geometric characteristics.

where w_c [m] is the channel width, and w_p [m] is the wall width.

This model includes several practical considerations and multiphase working fluid analysis, as discussed in [17]. So, the total entropy generation rate ($\dot{S}_{gen}$ [W/K]) of an RMCHS is described by

$$\dot{S}_{gen}(\alpha_c, \beta) = \frac{\dot{Q}_d^2}{T_a} \frac{R_{eq}(\alpha_c, \beta)}{T_i(\alpha_c, \beta)} + \frac{G_d}{T_a} \Delta P(\alpha_c, \beta), \qquad (2)$$

where $\dot{Q}_d$ [W] is the total heat power dissipated by the device, and R_{eq} [K/W] is the equivalent thermal resistance. Moreover, T_a [K] and T_i [K] are the surrounding and interface temperatures. G_d [m^3/s] is the volume flow rate, and ΔP [Pa] is the total pressure drop. Since T_i is calculated as

$$T_i(\alpha_c, \beta) = T_a + \dot{Q}_d R_{eq}(\alpha_c, \beta), \qquad (3)$$

the geometrical parameters α_c and β are then defined as

$$\alpha_c = \frac{2w_c}{h_c} \quad \text{and} \quad \beta = \frac{w_c}{w_p}. \qquad (4)$$

2) HEAT TRANSFER ASSUMPTIONS OF THE RMCHS MODEL
The heat transfer contribution is described by the first term of the model in (2), considering the next operative assumptions:
(a) RMCHS manages the transfer of the thermal energy from the electronic device to the fluid flow in the

microchannels through a steady heat flux, entered from the bottom plate up to the top.
(b) Radiation heat transfer vanishes in the top plate.
(c) Thermal contraction and dispersion due to different heat exchange areas are neglected.

3) MASS TRANSFER ASSUMPTIONS OF THE RMCHS MODEL
The second term in (2) describes the mass flow transfer contribution with the following assumptions:
(a) Steady thermophysical properties of the fluid flow are used in the RMCHS.
(b) Steady fluid flow and hydrodynamic are completely developed.
(c) Fluid flow is in the laminar regime. The transition and turbulent regimes are dismissed.

Remainder assumptions are related to the material and geometry being used in the RMCHS manufacture. These assumptions allowed finding the heat sink and thermal interface characteristics, which are considered macroscopically isotropic and excellent thermal conductors. Besides, they specify the relations among the heat sink, thermal interface, and electronic device areas. Therefore, the minimal area of the heat sink base ($A_{hs} = W_D \times L_D$) must be larger than or equal to the electronic device area (A_{ed}). Otherwise, the thermal interface area must be equal to the electronic device area ($A_{ti} = A_{ed}$). For further details, an in-deep analysis of the RMCHS model is addressed by Cruz-Duarte *et al.* in [17], [30].

B. OPTIMIZATION ALGORITHMS
This section presents fundamental concepts about the applied optimization algorithms (LM and MOAs). At first, three general definitions are given to support the used optimization algorithms.

Definition 1: Let $\mathcal{X}^n = \{\vec{x}_1^n, \vec{x}_2^n, \dots, \vec{x}_M^n\}$ be a finite set of candidate solutions for an optimization problem in $\mathbb{R}^D$ with an objective function given by $f : \mathbb{R}^D \to \mathbb{R}$. D is the dimensionality of the problem, and M is the number of candidate solutions. Thus, $\vec{x}_m^n = (x_{m,1}^n, x_{m,2}^n, \dots, x_{m,D}^n)^{\mathsf{T}}$ represents the m-th candidate in $\mathbb{R}^D$ at the time n under a maximum number of iterations N.

Definition 2: Let $\vec{x}_*^n \in \mathcal{X}^n$ be the best solution found at the n-th iteration,

$$\vec{x}_*^n = \underset{\mathcal{X}^n \cup \vec{x}_*}{\arg\inf} \left(f(\mathcal{X}^n) \cup f(\vec{x}_*^{n-1}) \right), \qquad (5)$$

where $f(\mathcal{X}^n) = \{f(\vec{x}_1^n), f(\vec{x}_2^n), \dots, f(\vec{x}_M^n)\}$.

Definition 3: Let $\mathcal{X}^{n+1}$ represent a finite set of new candidate solutions. Each new candidate $\vec{x}_m^{n+1}$ is obtained through an iterative procedure, namely, the optimization algorithm.

1) ELECTROMAGNETIC FIELD OPTIMIZATION
Electromagnetic Field Optimization (EFO) is a global optimization algorithm proposed by Abedinpourshotor-ban *et al.* [25]. It is a method inspired by the electromagnets

---

Algorithm 1 Electromagnetic Field Optimization (EFO)

Input: $f : \mathbb{R}^D \to \mathbb{R}$, $M > 2$, $\{P_r, P_p\} \in (0.1, 0.4)$, $M_p \in (0.05, 0.1)$, $M_n \in (0.4, 0.5)$, $N \gg 1$, and other stopping criteria

Output: $\vec{x}_*^n$

1: Initialize $\mathfrak{X}^0$, find $\vec{x}_*^0$ using Definition 2, and $n \leftarrow 0$.
2: **repeat**
3:      Update $\mathfrak{X}^{n+1}$ using (6).   ▷ Attraction/Repulsion
4:      Find $\vec{x}_*^{n+1}$ using Definition 2 and $n \leftarrow n + 1$.
5: **until** ($n < N$) & (Stopping criteria are not reached)

Algorithm 2 Unified Particle Swarm Optimization (UPSO)

Input: $f : \mathbb{R}^D \to \mathbb{R}$, $M > 2$, $\{u, \chi\} \in (0, 1)$, $\phi_1 + \phi_2 > 4$, $N \gg 1$, topology for $\mathfrak{Q}$, and other stopping criteria

Output: $\vec{x}_*^n$

1: Initialize $\mathfrak{X}^0$ and $\mathfrak{V}^0$, find $\vec{x}_*^0$ (Definition 2), and $n \leftarrow 0$.
2: **repeat**
3:      Find $\vec{x}_*^n$ using Definition 2.
4:      Find $\vec{x}_{m,l*}^n$ using Definition 6.
5:      Find $\vec{x}_{m,*}^n$ using Definition 7.
6:      Determine $\mathfrak{X}^{n+1}$ with (9) and (10),   ▷ Swarm Dynamic
7:      $n \leftarrow n + 1$.
8: **until** ($n < N$) & (Stopping criteria are not reached)

---

interaction, considering the magnets polarity in the search space. The electromagnets are classified through three interaction fields (positive, negative, and neutral), where attraction and repulsion forces lead the particles to the target.

Definition 4: Let $\mathfrak{P}_{pos}^n = \{\vec{x}_{pos,1}^n, \vec{x}_{pos,2}^n, \ldots, \vec{x}_{pos,M_p}^n\}$, $\mathfrak{P}_{neg}^n = \{\vec{x}_{neg,1}^n, \vec{x}_{neg,2}^n, \ldots, \vec{x}_{neg,M_n}^n\}$, and $\mathfrak{P}_{neu}^n = \{\vec{x}_{neu,1}^n, \vec{x}_{neu,2}^n, \ldots, \vec{x}_{neu,M-(M_p+M_n)}^n\}$ be the positive (*pos*), negative (*neg*), and neutral (*neu*) subpopulation fields. According to the fitness, these fields are classified, sorting the population $\mathfrak{X}^n$ from best (positives) to worst (negatives). Where $\{\mathfrak{P}_{pos}^n, \mathfrak{P}_{neu}^n, \mathfrak{P}_{neg}^n\} \subseteq \mathfrak{X}^n$. M_p and M_n are the subpopulations sizes of electromagnets in the positive and negative fields, respectively. Besides, $\vec{x}_m^{n+1}$ is obtained from (6), by the linear combination of $\vec{x}_{pos,m}^n \in \mathfrak{P}_{pos}^n$, $\vec{x}_{neg,m}^n \in \mathfrak{P}_{neg}^n$, and $\vec{x}_{neu,m}^n \in \mathfrak{P}_{neu}^n$ vectors.

The interactions among the electromagnets generate new positions according to

$$\vec{x}_m^{n+1} = \vec{x}_{neu,m}^n + \varphi r_f(\vec{x}_{pos,m}^n - \vec{x}_{neu,m}^n) \\ - r_f(\vec{x}_{neg,m}^n - \vec{x}_{neu,m}^n), \quad (6)$$

where $\vec{x}_m^{n+1}$ is the new electromagnet position for the design variable. Likewise, r_f is a random variable with a uniform distribution $\mathcal{U}(0, 1)$, and φ is the ratio of the attraction and repulsion forces, using the golden ratio $\varphi = (1 + \sqrt{5})/2$. EFO algorithm includes complementary parameters as the probability of selecting electromagnets from the positive field P_p without being modified. Besides, P_r is the probability of changing one electromagnet by another randomly generated. EFO method is synthesized in Algorithm 1.

2) UNIFIED PARTICLE SWARM OPTIMIZATION

Unified Particle Swarm Optimization (UPSO), proposed by Parsopoulos and Vrahatis in 2004 [26], enhances the popular Particle Swarm Optimization (PSO) algorithm [31]. It is a swarm intelligence-based technique widely used in engineering design applications [32]–[34]. All swarm particles have two essential components: position ($\vec{x}_m^n \in \mathfrak{X}^n$) and velocity ($\vec{v}_m^n \in \mathfrak{V}^n$), described through the following definitions.

Definition 5: Let $\mathfrak{Q}_m^n \subseteq \mathfrak{X}^n$ be the neighborhood of the m-th candidate solution $\vec{x}_m^n$, at the time n, and disposing of a given topology, *e.g.*, $\mathfrak{Q}_m^n = \{\vec{x}_{m-1}^n, \vec{x}_m^n, \vec{x}_{m+1}^n\}$.

Definition 6: Let $\vec{x}_{m,l*}^n \in \mathfrak{Q}_m^n$ be the best candidate solution in the neighborhood $\mathfrak{Q}_m^n$, defined by

$$\vec{x}_{m,l*}^n = \arg\inf\left(f(\mathfrak{Q}_m^n) \cup \{f(\vec{x}_{m,l*}^{n-1})\}\right). \quad (7)$$

Definition 7: Let $\vec{x}_{m,*}^n$ be the best solution, where the m-th particle has been found until the time n, *i.e.*,

$$\vec{x}_{m,*}^n = \arg\inf\left(f(\vec{x}_{m,*}^n), f(\vec{x}_{m,*}^{n-1})\right). \quad (8)$$

Therefore, the new position for each particle $\vec{x}_m^{n+1}$ is obtained by

$$\vec{x}_m^{n+1} = \vec{x}_m^n + \vec{v}_m^{n+1}, \quad (9)$$

since the total velocity ($\vec{v}_m^{n+1}$) is calculated as a weighted sum between the global ($\vec{G}_m^{n+1}$) and local ($\vec{L}_m^{n+1}$) velocities

$$\vec{v}_m^{n+1} = (1 - u) \odot \vec{L}_m^{n+1} + u \odot \vec{G}_m^{n+1}, \quad (10)$$

where $u \in [0, 1]$ is the unification factor to balance the global and local displacement contributions. The velocity components are then obtained as

$$\vec{G}_m^{n+1} = \chi[\vec{v}_m^n + \phi_1 \vec{r}_1 \odot (\vec{x}_{m,*}^n - \vec{x}_m^n) + \phi_2 \vec{r}_2 \odot (\vec{x}_*^n - \vec{x}_m^n)], \quad (11)$$

$$\vec{L}_m^{n+1} = \chi[\vec{v}_m^n + \phi_1 \vec{r}_3 \odot (\vec{x}_{m,*}^n - \vec{x}_m^n) + \phi_2 \vec{r}_4 \odot (\vec{x}_{m,l*}^n - \vec{x}_m^n)], \quad (12)$$

where $\chi \in (0, 1]$ is the constriction factor, $\odot$ is the Hadamard product (*i.e.*, element-wise multiplication), $\vec{v}_m^n$ and $\vec{x}_m^n$ are the current velocity and position for the m-th particle, ϕ_1 and ϕ_2 are the self and swarm confidence coefficients. Besides, $\vec{r}_1$, $\vec{r}_2$, $\vec{r}_3$, and $\vec{r}_4$ are vectors of identically independent distributed (i.i.d.) random variables with a uniform distribution $\mathcal{U}(0, 1)$; $\vec{x}_{m,*}^n$, $\vec{x}_{m,l*}^n$, and $\vec{x}_*^n$ are the best position of each particle (Definition 7), at each neighborhood (Definition 6), and in the entire swarm (Definition 2), respectively. Algorithm 2 summarizes the UPSO method.

3) DIFFERENTIAL EVOLUTION

Differential Evolution (DE), developed by Storn and Price in 1996 [27], is a stochastic population-based optimization algorithm. Three primary stages, known as a mutation,

---

Algorithm 3 Differential Evolution (DE)

Input: $f : \mathbb{R}^D \to \mathbb{R}$, $M > 3$, $C_p \in (0, 1)$, $D_w \in (0, 2)$, $N \gg 1$, and other stopping criteria

Output: $\vec{x}_*^n$
 1: Initialize $\mathcal{X}^0$, find $\vec{x}_*^0$ using Definition 2, and $n \leftarrow 0$.
 2: **repeat**
 3:     Determine $\vec{v}_m^{n+1}$ using (13).   ▷ Mutation
 4:     Determine $\vec{u}_m^{n+1}$ using (14).   ▷ Crossover
 5:     Determine $\mathcal{X}^{n+1}$ using Definition 15.
 6:     Find $\vec{x}_*^{n+1}$ using Definition 2, $n \leftarrow n + 1$.   ▷
     Selection
 7: **until** $(n < N)$ & (Stopping criteria are not reached)

---

crossover, and selection, develop the optimization process for real-valued functions. Therefore, it uses three vectors, named mutated, target, and trial vector, respectively. Each mutated vector $\vec{v}_m^{n+1}$ is obtained by a linear combination

$$\vec{v}_m^{n+1} = \vec{x}_{z_1}^n + D_w(\vec{x}_{z_2}^n - \vec{x}_{z_3}^n), \qquad (13)$$

where z_1, z_2, and z_3 are random and mutually different integers $\mathcal{U}(1, M)$, even with the index m. The population size M must be larger than three. $D_w \in [0, 2]$ represents the differential weight, being real and constant during the optimization process. In this study, a binomial crossover-type was used. Therefore, the trial vectors $\vec{u}_m^{n+1}$ are generated by taking elements randomly either from mutated or from the current element in the population

$$\vec{u}_m^{n+1} = \begin{cases} \vec{v}_{m,l}^{n+1} & \text{if } R_u \leq C_p \vee l = I_u(m) \\ \vec{x}_{m,l}^n & \text{if } R_u > C_p \vee l \neq I_u(m), \end{cases} \qquad (14)$$

where $l = 1, 2, \ldots, D$, being D the dimensionality, R_u is generated with the uniform distribution $\mathcal{U}(0, 1)$, and $I_u \sim \mathcal{U}_I(1, D)$ is an integer randomly selected from l. $C_p \in [0, 1]$ is the crossover factor. In the selection stage, the trial and target vectors are compared to keep the best actual solutions. The selection stage of $\vec{x}_m^{n+1}$ is defined by

$$\vec{x}_m^{n+1} = \begin{cases} \vec{u}_m^{n+1}, & \text{if } f(\vec{u}_m^{n+1}) \leq f(\vec{x}_m^n) \\ \vec{x}_m^n, & \text{otherwise.} \end{cases} \qquad (15)$$

Algorithm 3 summarizes the overall DE method.

4) SPIRAL OPTIMIZATION

Spiral Optimization (SO) is a direct-solving metaheuristic procedure based on the logarithmic spiral dynamic [35], [36]. This numerical process rotates a set of points around a reference center point, following a logarithmic spiral trajectory. The reference is iteratively updated using a fitness criterion, *i.e.,* a location $(\vec{x}_*^n)$ given by an objective function $f(\vec{x})$, $\vec{x} \in \mathbb{R}^D$. Such an idea is formulated using Definitions 1 to 3, such as

$$\vec{x}_m^{n+1} = r\mathbf{R}_D(\theta)\vec{x}_m^n - (r\mathbf{R}_D(\theta) - \mathbf{I}_D)\vec{x}_*^n, \qquad (16)$$

where $\mathbf{I}_D \in \mathbb{R}^{D \times D}$ is the identity matrix, $r \in (0, 1)$, and $\theta \in (0, 2\pi)$ are the control parameters of the spiral

---

Algorithm 4 Spiral Optimization (SO)

Input: $f : \mathbb{R}^D \to \mathbb{R}$, $M > 2$, $\theta \in (0, 2\pi)$, $r \in (0, 1)$, $N \gg 1$, and other stopping criteria

Output: $\vec{x}_*^n$
 1: Determine $\mathbf{R}_D(\theta)$ using (17).
 2: Initialize $\mathcal{X}^0$, find $\vec{x}_*^0$ using Definition 2, $n \leftarrow 0$.
 3: **repeat**
 4:     Update $\mathcal{X}^{n+1}$ using (16).   ▷ Spiral Dynamic
 5:     Find $\vec{x}_*^{n+1}$ using Definition 2, $n \leftarrow n + 1$.
 6: **until** $(n < N)$ & (Stopping criteria are not reached)

---

dynamics, representing the convergence rate and the rotation angle between an m-th point $(\vec{x}_m^n)$ and the center point $(\vec{x}_*^n)$. Likewise, $\mathbf{R}_D(\theta) \in \mathbb{R}^{D \times D}$ is the rotation matrix defined by the product of all combinations of 2D rotation matrices

$$\mathbf{R}_D(\theta) = \prod_{k=1}^{K} \mathbf{R}(\theta_k) = \prod_{k=1}^{K} e^{\theta \mathbf{L}_k} \in \mathbf{R}^{D \times D}, \qquad (17)$$

where $\mathbf{L}_k = \hat{u} \otimes \hat{v} - \hat{v} \otimes \hat{u}$ is the skew-symmetric matrix generator that follows the Euler-Rodrigues rotation formula [37]. Since the k-th plane, $k \in \{1, 2, \ldots, K\}$, is formed by a vector pair $\{\hat{u}, \hat{v}\}$ from the canonical basis of $\mathbb{R}^D$, $\{\hat{u}, \hat{v}\} \in \{\hat{e}_1, \hat{e}_2, \ldots, \hat{e}_D\}$, $\otimes$ is the outer product or the tensor product of two column vectors represented by the multiplication $\hat{u}\,\hat{v}^\mathsf{T}$, and $\binom{D}{2}$ is the number of planes. The SO is summarized in Algorithm 4.

5) SIMULATED ANNEALING

Simulated Annealing (SA), presented by Kirkpatrick *et al.* in 1983 [29], is a multivariate and combinatorial optimization algorithm based on statistical mechanics and thermal equilibrium searching.

Definition 8: Let $\Delta f(\vec{x}_m^n)$ be the difference between m-th energetic status of candidate solutions, $f(\vec{x}_m^{n+1})$ and $f(\vec{x}_m^n)$, at the time n.

From the energetic status $f(\vec{x}_m^n)$ of $\vec{x}_m^n$, the next candidate solution $\vec{x}_m^{n+1}$ is selected by the Metropolis criterion [38]

$$P\left\{f(\vec{x}_m^{n+1})\right\} = \text{arginf}\left\{1, \exp\left(\frac{\Delta f(\vec{x}_m^n)}{K_B T_0}\right)\right\}, \qquad (18)$$

where k_B is the Boltzmann constant and T_0 is the temperature control variable. Other control variables include the number of complete cycles p_c, temperature decreasing factor $c \in (0, 1)$, and the number of states Ψ. SA is presented in Algorithm 5.

6) LEVENBERG-MARQUARDT ALGORITHM IN THE IHTP SOLUTION PROCESS

Levenberg-Marquardt (LM) is the most common gradient-based algorithm used to solve the IHTP and is usually combined with the Ordinary Least Square Norm (OLSN) as the cost function. The IHTP solved by the LM also uses the framework previously mentioned [9]. At the beginning of the DP phase, the physical model must be clearly analyzed

---

Algorithm 5 Simulated Annealing (SA)

Input: $f : \mathbb{R}^D \to \mathbb{R}$, $M > 1$, $N_{tem} \gg 1$, $T_0 > 1000$, $p_c \in (1, 10)$, $c \in (0, 1)$, $N \gg 1$, and other stopping criteria
Output: $\vec{x}_*^n$
1: Initialize $\mathfrak{X}^0$, find $\vec{x}_*^0$ using Definition 2, and $n \leftarrow 0$.
2: **repeat**
3:      Determine $\mathfrak{X}^{n+1}$ using Definition 8 and (18) $\triangleright$ Annealing Process
4:      Update $p \leftarrow p + 1$ and $T_0 \leftarrow cT_0$
5:      Find $\vec{x}_*^{n+1}$ using Definition 2 and $n \leftarrow n + 1$.
6: **until** $(n < N)$ & (Stopping criteria are not reached)

Algorithm 6 Levenberg-Marquardt (LM)

Input: $f : \mathbb{R}^D \to \mathbb{R}$, $\vec{P}^0$, $\Phi^0 \gg 0$, $c_1 \in (0, 1)$, $c_2 \in (1, 10)$, $N \gg 1$, and other stopping criteria
Output: $\vec{x}_*^n$
1: Initialize $\mathfrak{X}^0$, find $\vec{x}_*^0$ using Definition 2, and $n \leftarrow 0$.
2: **repeat**
3:      Determine $\mathfrak{X}^{n+1}$ using (23) $\triangleright$ LM Rule
4:      Update Φ^n using (24)
5:      Find $\vec{x}_*^{n+1}$ using Definition 2 and $n \leftarrow n + 1$.
6: **until** $(n < N)$ & (Stopping criteria are not reached)

---

as a cause-and-effect problem. In heat transfer, the causes are usually the thermal sources, and the effects can be the output temperature profiles $T(x, t)$ from the model equations. Next, the IP statement describes how the causes can be estimated knowing the corresponding effects in a physical model. Usually, diversified data is required, as temperature measurements several positions from single or multiple sensors at various periods. The cost function is given by the OLSN, such as

$$S(\vec{P}) = [\vec{Y} - \hat{\vec{Y}}(\vec{P})]^\mathsf{T} [\vec{Y} - \hat{\vec{Y}}(\vec{P})], \tag{19}$$

where $\vec{P} \in \mathbb{R}^D$ is the vector of unknown parameters to be estimated, Y and $\hat{Y}(\vec{P})$ are measured and estimated data, respectively. Therefore, the DP and IP require of efficient optimization algorithm to support a dependable IHTP solution. In particular, the iterative LM method requires computing the gradient of the $S(\vec{P})$, $\nabla S(\vec{P})$, which tends to zero while finding the minima (or maxima)

$$\nabla S(\vec{P}) = -2 \frac{\partial \hat{\vec{Y}}^\mathsf{T}(\vec{P})}{\partial \vec{P}} [\vec{Y} - \hat{\vec{Y}}(\vec{P})] = -2\hat{J}^\mathsf{T}(\vec{P})[\vec{Y} - \hat{\vec{Y}}(\vec{P})], \tag{20}$$

where $\vec{J}(\vec{P}) \in \mathbb{R}^{L \times D}$ is the Jacobian matrix. In the linear cases, the Jacobian matrix is independent of unknown parameters, and a closed solution can be found by $\hat{\vec{P}} = (\vec{J}^\mathsf{T} J)^{-1} \vec{J}^\mathsf{T} \vec{Y}$. But, in the nonlinear and general cases, $\hat{\vec{Y}}(\vec{P})$ is linearized through the first-order Taylor series

$$\hat{\vec{Y}}(\vec{P}) = \hat{\vec{Y}}(\vec{P}^n) + \hat{J}^n(\vec{P} - \vec{P}^n), \tag{21}$$

expanded around $\vec{P}^n$ to define the iterative LM rule

$$\vec{P}^{n+1} = \vec{P}^n + [(\hat{J}^n)^\mathsf{T} \hat{J}^n]^{-1} (\hat{J}^n)^\mathsf{T} [\vec{Y} - \hat{\vec{Y}}(\vec{P}^n)]. \tag{22}$$

Usually, the IHTPs are ill-posed because of $|\vec{J}^\mathsf{T} \vec{J}| \approx 0$. However, these method instabilities can be avoided using a regularization damping term Φ and the definite positive matrix Ω. The LM formula is finally stated as

$$\vec{P}^{n+1} = \vec{P}^n + [(\hat{J}^n)^\mathsf{T} \hat{J}^n + \Phi^n \Omega^n]^{-1} (\hat{J}^n)^\mathsf{T} [\vec{Y} - \hat{\vec{Y}}(\vec{P}^n)]. \tag{23}$$

It is important to remark that Φ and Ω may vary during the iterative process, and their initial values are essential

for LM convergence. In this study, to improve LM performance, the Ω^n matrix is computed from the diagonal matrix of $[(\vec{J}^n)^\mathsf{T} \vec{J}^n]$, and the initial Φ^0 value is chosen between $[10^3, 10^6]$. The Φ^n value is iteratively updated by

$$\Phi^{n+1} = \begin{cases} c_1 \Phi^n, & \text{if } f(\vec{x}_m^{n+1}) \le f(\vec{x}_m^n) \\ c_2 \Phi^n, & \text{otherwise. }, \end{cases} \tag{24}$$

where the constants $c_1 \in (0, 1)$ and $c_2 \in (1, 10)$ dynamically help to increase or decrease the Φ^n value, respectively.

The typical stopping criterion used with the IHTP analysis and LM, estimates the precision of the parameters between two consecutive iterations by $\|\vec{P}^{n+1} - \vec{P}^n\|_2 < \epsilon$, where ϵ is user-defined. Due to premature convergence issues in using this last criterion, a robust stopping criterion is proposed in our implementation, presented in Section III-D. Finally, an optimal solution is achieved when the procedure converges, fulfilling the stopping criteria. Algorithm 6 summarizes the LM method.

III. METHODOLOGY

All experiments were run on an Acer Aspire VX15 model VX5-591G, with an Intel® Core™ i7-7700HQ CPU at 2.8GHz, 16GB RAM, and Windows 10 OS. The configuration parameters and their corresponding intervals are different for traditional or nontraditional algorithms, depending on their nature and mathematical support. Table 4 shows the referenced intervals and selected parameters for all implemented MOAs in the numerical analysis.

A benchmarking routine over the LM and the MOAs was applied before solving the IHTP application. This benchmarking was based on testing parameter combinations exhaustively. The processing times, the optimal and minimal least squared errors for all standard functions are computed to determine the most suitable parameters combination for each algorithm. The benchmarking used ten well-known standard functions, which are shown in Table 1. These allow parametrizing and characterizing each algorithm configuration even through convergence rate and error values (*e.g.*, relative, absolute, or root mean square error). The benchmark functions were selected based on their mathematical similarity with the RMCHS model. Estimated MOAs performance needed to repeat each study case 100 times with a maximum

TABLE 1. Selected standard benchmark functions [39].

Label	Function	Dimensions
f_{01}	Ackley	2, 5, 10
f_{02}	Bird	2
f_{03}	Bukin 6	2
f_{04}	Carrom Table	2
f_{05}	Chichinadze	2
f_{06}	Goldstein-Price	2
f_{07}	Helical Valley	3
f_{08}	Plateau	2, 5, 10
f_{09}	Rosenbrock	2, 5, 10
f_{10}	Test Tube holder	2

TABLE 2. Design variables vectors (θ_I) for each tested strategy and sequential order (sensitivity influence) of estimation and optimization in serial and parallel strategies.

Strategy	Estimation Sequence	$\vec{\theta}_I^\intercal$
Serial	Geometry (First step)	(α_c, β) (2-tuple)
	Material (Second step)	(k_m, ρ_m) (2-tuple)
	Fluid (Third step)	(k_f, ρ_f, ν, c_p) (4-tuple)
Parallel	Multiparametric	$(\alpha_c, \beta, k_m, \rho_m, k_f, \rho_f, \nu, c_p)$

TABLE 3. Average thermophysical properties of the material and fluid used in the RMCHS model.

	Thermophysical properties					
	k_m [W/m^2·K]	ρ_m [kg/m^3]	k_f [W/m^2·K]	ρ_f [kg/m^3]	ν [m^2/s]	c_p [J/kg·K]
Aluminum	237.00	2707.0	–	–	–	–
Air	–	–	0.0261	1.1614	1.5800	1007.0

of 1000 iterations, guaranteeing a robust and statistically reliable evaluation test.

For all standard functions, the evaluations were performed in 2-D, varying the population sizes $M \in \{10, 25, 50, 75, 100\}$. Additionally, the Ackley, Plateau, and Rosenbrock standard functions were evaluated for 5 and 10 dimensions.

However, the randomness nature of all optimization metaheuristic methods rends a fair evaluation a challenge. For this reason, parametric and nonparametric statistical tests were used to diversify the evaluation to obtain the tuning parameters for the most suitable algorithm in the application. Hence, the nonparametric Wilcoxon-Mann-Whitney test was applied, ranking the parameters set previously determined by the benchmarking and completing the selection of the appropriate parameters. Complementarily, the evaluation task required applying the same operative conditions (*i.e.,* search space, stopping criteria, and constraints) to guarantee a fair comparison between the algorithms.
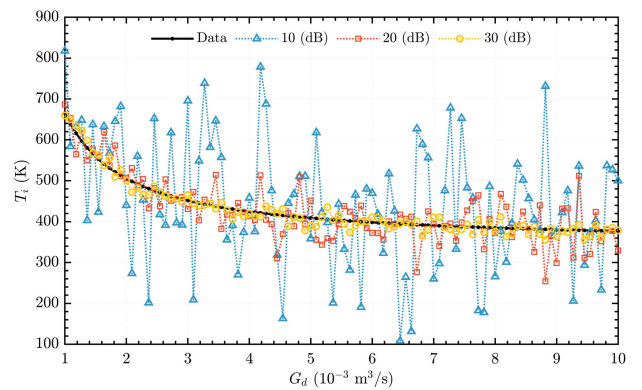
The MOAs are straightforwardly integrated into the process, evaluating the two solution strategies. A multiparametric strategy processes eight parameters (design variables) simultaneously, *i.e.,* estimation-optimization is performed in parallel (see Table 2). Moreover, a serial strategy deals with the sequence order to estimate and optimize parameters, starting with the most sensitive in the RMCHS model. For a more comprehensive analysis, three design tests related to parameters class are performed (*i.e.,* geometry, building material, and working fluid parameters test). Table 2 summarizes the parameters used in the proposed design tests: the geometrical parameters $10^{-3} \leq \alpha_c \leq 10^{-2}$ and $1 \leq \beta \leq 5$ [17] given by (4), the material parameters with the conductivity (k_m [W/m^2·K]) and density (ρ_m [kg/m^3]), and the fluid parameters considering the conductivity (k_f [W/m^2·K]), density (ρ_f [kg/m^3]), kinematic viscosity (ν [m^2/s]), and specific heat (c_p [J/kg·K]). For simulation purposes, Aluminum (Al) was the material studied to build the RMCHS body, and the working fluid air (Air) was used as the active substance [40]. Their thermophysical properties are given in Table 3. A minimum allowed SNR was identified to find a reliable and stable estimation in measurements. Fig. 3 presents three synthetic noisy temperature profiles, where three power levels (10, 20, and 30 dB of SNR) of Additive White Gaussian

FIGURE 3. Profile T_i (Interface Temperature) against G_d (Volume Flow Rate) with three distinct levels of SNR (in decibels).

Noise (AWGN) were added to the original signal (continuous plot). It is noteworthy that the noisiest profile is the signal with 10 dB of SNR. Subsequently, the IHTP inverse analysis development was based on five operative phases: Direct Problem, Inverse Problem, Iterative Procedure, Stopping Criteria, and Computational Algorithm. Fig. 4 shows a detailed flowchart of these phases, which are described next.

A. DIRECT PROBLEM

It assumes that all model parameters are known with sufficient accuracy to find the minimal entropy generation rate for an RMCHS model. It is represented by

$$\min_{(\vec{\theta}_D)} \{\dot{S}_{gen}(\vec{\theta}_D)\} = \arg\min \left\{ \dot{Q}_d^2 \frac{R_{eq}(\vec{\theta}_D)}{T_a T_i(\vec{\theta}_D)} + \frac{G_d}{T_a} \Delta P(\vec{\theta}_D) \right\}$$

$$\text{subject to} \begin{cases} g_1(\vec{\theta}_D) = \alpha_c - 1 \leq 0 \\ g_2(\vec{\theta}_D) = 1 - \beta \leq 0, \end{cases} \quad (25)$$

where $\vec{\theta}_D = (\alpha_c, \beta)^\intercal$. This phase includes three main blocks (red dashed box in Fig. 4) the RMCHS mathematical model, tested optimization methods, and optimal results.
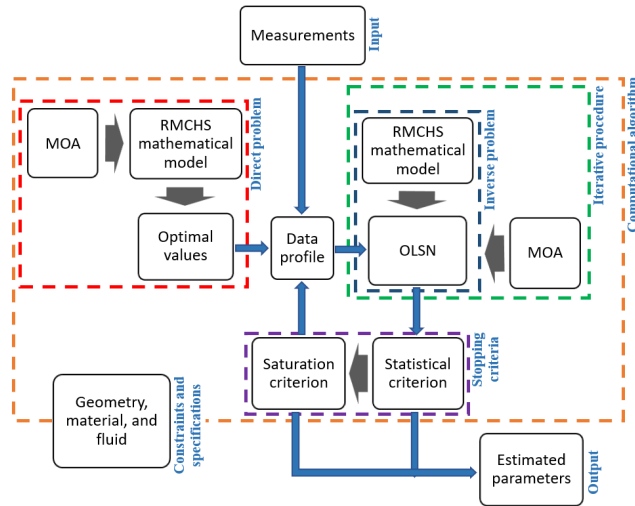
FIGURE 4. Proposed five-phases IHTP inverse analysis applied into the Rectangular Microchannel Heat Sink (RMCHS) design. The Metaheuristic Optimization Algorithm (MOA) is the fundamental block for the direct and inverse problems phases. The cost function is based on the Ordinary Least Square Norm (OLSN), guided by the saturation and statistical stopping criteria.

B. INVERSE PROBLEM

It considers that all remainder model parameters are known with sufficient accuracy to estimate any RMCHS model parameter. This estimation is conducted by minimizing the sum of squared residuals $S(\vec{\theta}_I)$

$$\min_{(\vec{\theta}_I)} \{S(\vec{\theta}_I)\} = \arg\inf \left\{ \sum_{i=1}^{L} \left[T_i(G_d) - \hat{T}_i(\vec{\theta}_I, G_d) \right]^2 \right\}, \quad (26)$$

where $\vec{\theta}_I$ is given in Table 2 and subject to identical constraints in (25). $\hat{T}_i$ was calculated using (3) and linked to the $\dot{S}_{gen}$ by R_{eq}. Fig. 3 shows the temperature profiles T_i (sensor measurements) as a function of the volume flow rate G_d, data required to solve the IP. Fig. 4 (blue dashed boxes) presents the functions associated with the IP estimation process: the RMCHS mathematical model and the OLSN.

C. ITERATIVE PROCEDURE

The recurrent minimization of the OLSN was used to achieve an acceptable solution, leading to computing the sum of squared residuals

$$S(\vec{\theta}_I) = \sum_{i=1}^{L} \left[T_i(G_d) - \hat{T}_i(\vec{\theta}_I, G_d) \right]^2, \quad (27)$$

where $T_i(G_d)$ is the observed response (variable measurements), $\hat{T}_i(\vec{\theta}_I, G_d)$ is the estimated temperature profile (fitted response or variable estimation) through the model using the same values of G_d in T_i for each i. D and L, represent the number of unknown parameters (dimensionality) and measurements (data length), respectively. For this study, $L \geq D$ guarantees an adequate estimation. Experimentally, $D = 8$ (maximal) and $L = 100$ were selected. Finally, the inverse problem is solved using the LM algorithm and proposed MOAs, see Fig. 4 (green dashed box).

D. STOPPING CRITERIA

Selected stopping criteria allow reaching stable solutions about nonsystematic errors (due to noise or disturbances) produced during the data acquisition. The first criterion was focused on the stagnation state, $m_{sat} \leq N$. The iterative process is stopped until it reaches a maximum number of iterations regardless of the current accuracy improvement. Next, the number of iterations m_{sat} is defined as the saturation condition. The stagnation criterion serves for fair comparisons because it also represents a fixed cost performance [41]. The second criterion is based on the statistical treatment of solutions at each iteration,

$$|f(\vec{\theta}_I)_n - \mu_{fn}| \leqslant \sigma_{fn}, \quad (28)$$

where μ_{fn} and σ_{fn} are the mean and standard deviation of historical fitness values at step n. This other useful criterion is a fixed target measure [41].

Fig. 4 (purple dashed box) includes both primary and secondary criteria.

E. COMPUTATIONAL ALGORITHM

A computational algorithm assembles the previous phases of the inverse analysis to obtain the general solution to the RMCHS design. Fig. 4 shows a flowchart with the IHTP solution phases as dashed boxes, coded as subroutines. Serial and parallel strategies are the main routines, where some SNR levels of noise were added in every proposed design test related to geometry, material, and fluid to verify method robustness. Each subroutine has associated one or more functional blocks, *e.g.,* RMCHS mathematical model, MOA code, cost function, and reference tuning values. Specifications and constraints for the model design are global and common for all subroutines implemented in the IHTP solution framework. Selected tuning parameters for MOAs are shown in Table 4, which were considered the initial values for each MOA during the estimation and optimization in the overall computational algorithm. The final used population size M also resulted from the benchmarking process over the preliminary metaheuristic algorithm analysis. Plus, note that the space dimensionality denoted by D depends on the number of design variables in the application.

F. NONPARAMETRIC EVALUATION TESTS

Three nonparametric tests of null hypothesis were used to obtain a robust method evaluation. They include the Wilcoxon-Mann-Whitney (Rank-sum) [42], [43], the Friedman [42], [44], and the Kruskal-Wallis [42] tests. The selected tests are counterparts of the ANOVA test family [42]. The nonparametric statistical tests are applied when the distribution data information is not available and cannot be assumed accurately. These tests require ranking the data calculations, ordinal samples (*i.e.,* sorted and ranked). Besides, the data samples must be independent, sometimes assuming the homoscedasticity with a corresponding correction factor. Such nonparametric tests are briefly described next and
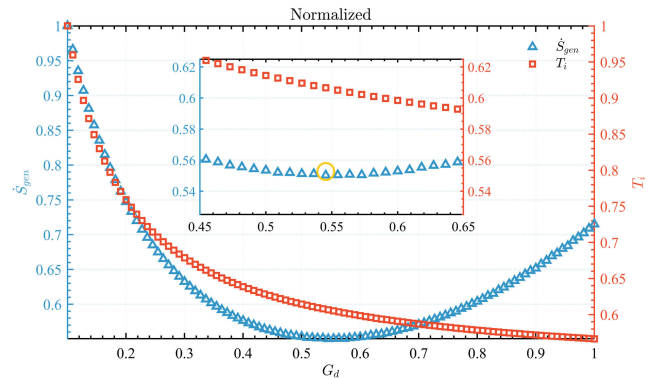
TABLE 4. Configuration parameters for optimization algorithms. *Coded algorithms are publicly available at https://github.com/batdraco/OAs.

Method	Parameter	Possible values		Selected values
		Lower	Upper	
LM	Φ^0	0.0000	10^6	10^3
	c_1	0.0000	1.0000	0.3500
	c_2	1.0000	10.000	2.8571
EFO	M	50.000	D	50.000
	M_p	0.0500	0.1000	0.1000
	M_n	0.4000	0.5000	0.4500
	P_p	0.1000	0.4000	0.2000
	P_r	0.1000	0.4000	0.3000
UPSO	M	D	100.00	25.000
	ϕ_1	1.0000	2.0000	2.0000
	ϕ_2	2.0000	3.0000	2.5000
	χ	0.0000	1.0000	0.6000
	u	0.0000	1.0000	0.5000
DE	M	D	100.00	25.000
	C_p	0.6000	1.0000	0.7000
	D_w	0.0000	2.0000	0.6000
SO	M	D	100.00	25.000
	θ	0.0000	6.2832	0.3927
	r	0.0000	1.0000	0.9500
SA	M	100.00	1000.0	100.00
	T_0	1000.0	10000	1400.0
	p_c	1.0000	10.000	1.0000
	c	0.0000	1.0000	0.6000

TABLE 5. Optimal reference values of the RMCHS model.

Test	α_c	β	N_c	G_d [m³/s]	$\dot{S}_{gen}$ [W/K]
Al+Air	3.61×10^{-3}	2.0739	373.00	5.45×10^{-3}	0.3787

FIGURE 5. Entropy generation rate ($\dot{S}_{gen}$) and interface temperature (T_i) profile as a Flow Volume Rate (G_d) function (normalized axes).

discussed in Section IV to determine the suitable solution strategy and optimization algorithm. The Wilcoxon–Mann–Whitney rank-sum is a test used to compare two performance results or samples, using a null hypothesis [42], [43]. The null hypothesis ($\mathfrak{H}_0$) is tested for verifying if data samples proceed from the identical distributions with equal medians or not. $\mathfrak{H}_0$ is a logical value that accepts ($\mathfrak{H}_0 = 0$) or rejects ($\mathfrak{H}_0 = 1$) the null hypothesis statement with a significance level of α_s and a probability of p-value. Succinctly, it analyzes and compares two distributions and their medians to determine if they are statistically and significantly similar or different from each other. Contrarily, the Friedman is a test used to compare multiple outcomes at once [42], [44]. Just as the Wilcoxon–Mann–Whitney test, the null hypothesis is based on all samples belonging to the same distribution with their medians equal, and the samples are mutually independent. In the Friedman test, a p-value about 1.0 indicates that the null hypothesis is accepted (*i.e.,* all algorithms' results are comparatively similar; otherwise, they are significantly different). Alike, the Kruskal-Wallis is another test used to compare multiple samples [42]. This last test behaves operatively similar to the Wilcoxon–Mann–Whitney test, but including more than two samples. It is noteworthy that the three nonparametric tests involve the p-value, α_s, and the rank-sum to analyze the distributions. Besides, this method can also rank the results using the statistic μ-rank as the Friedman test. Therefore, these nonparametric tests were selected because their results are entirely compatible, confirming the same hypothesis. Such tests were efficiently used to rank strategies and qualitatively compare the proposed optimization algorithms.

IV. NUMERICAL RESULTS

The solution of the stated optimization problem (*i.e.,* DP) is obtained by computing the optimal geometrical parameters α_c and β (consequently, N_c), both functions of G_d minimizing $\dot{S}_{gen}$, (25). Table 5 gives the optimization results of the RMCHS modeling, considering the references for the following analyses. Such data allow determining both behaviors, the T_i (red color and square marker) and $\dot{S}_{gen}$ (blue color and triangle marker) as functions of G_d, as shown in Fig. 5. The minimal value of $\dot{S}_{gen}$ is found between 5×10^{-3} and 6×10^{-3} [m³/s] of G_d, confirming the obtained values with the optimization process graphically, see Table 5. Moreover, the referencing curve T_i-G_d in Fig. 5 permits verifying the accuracy of each estimated parameter and performance test.

A. COMPARATIVE SERIAL STRATEGY - PARALLEL STRATEGY

The entropy generation rate ($\dot{S}_{gen}$) profile was plotted for the original data (without noise) and noise-contaminated signal at several SNR levels (10, 20, and 30 dB) to compare the serial and parallel strategies. Fig. 6 shows the estimated profile $\dot{S}_{gen}$ using the strategies serial and parallel without adding AWGN, *i.e.,* these data match the references shown in Fig. 5. The previous result reveals an intrinsic offset during the estimation process while applying each MOAs. The differences between the results given by strategies serial and parallel are manifest. Most MOAs adjust the data with minimal errors using the serial strategy.

Nevertheless, UPSO, DE, and SO gave minor errors in the adjusting process; the most accurate were DE and UPSO using the parallel strategy. Fig. 7 shows orders of magnitude between 10^{-2} and 10^{-1} to find the required OLSN minimal value (*i.e.,* $\dot{S}_{gen}$ minimal) employing the serial strategy.
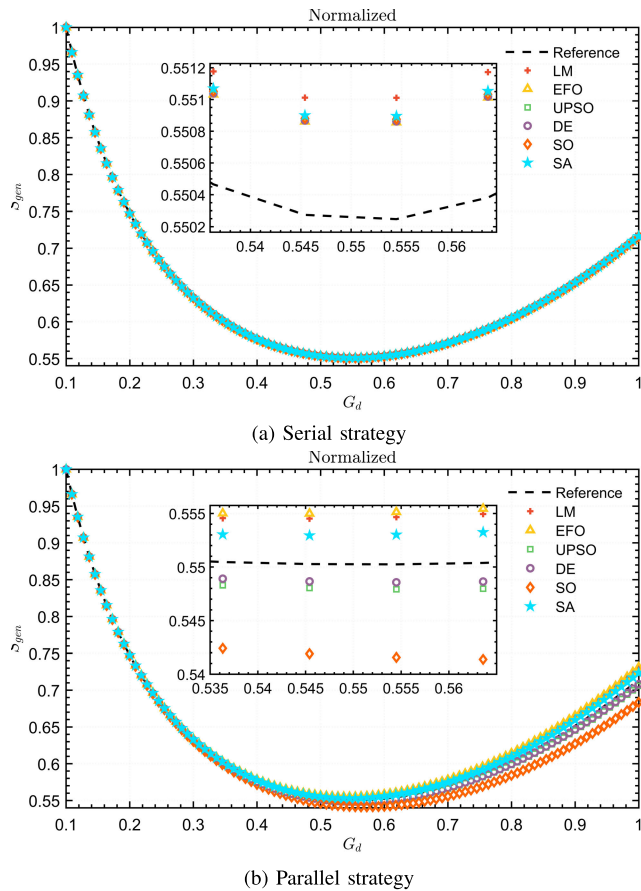
(a) Serial strategy

(b) Parallel strategy

FIGURE 6. Entropy generation rate ($\dot{S}_{gen}$) profile estimation without SNR of AWGN by using the (a) serial strategy and (b) parallel strategy (normalized axes).

(a) Serial strategy

(b) Parallel strategy

FIGURE 7. Relative errors for geometrical parameters (α_c and β), Volume Flow Rate (G_d), and Entropy Generation Rate ($\dot{S}_{gen}$) for 30 dB of AWGN using the (a) serial and (b) parallel strategy.

TABLE 6. Wilcoxon–Mann–Whitney test results for serial and parallel strategies comparison with a significance level of $\alpha_S = 0.01$.

Comparison	*p*-value	$\mathfrak{H}_0$	α_S	Rank-sum
Parallel vs. Serial	0.5487	0	0.01	9217.0

TABLE 7. Friedman and Kruskal-Wallis test results in ranking the serial and parallel strategies with a significance level of $\alpha_S = 0.01$.

Evaluation test	*p*-value	Statistics	Ranking	
			Serial strategy	Parallel strategy
Friedman	0.9553	μ-ranks	**2.4948**	2.5052
		σ-ranks	1.2883	1.2883
Kruskal-Wallis	0.9028	μ-rank	**96.010**	96.990

Likewise, orders of magnitude between and 10^2 were obtained during the OLSN minimization using the parallel strategy. It is noteworthy that serial strategy has lower variations than the parallel for every tested SNR level. Furthermore, Tables 8 and 9 provide precise data to numerically determine that the serial strategy is more accurate than the parallel strategy, analyzing the reduced errors between the reference and estimated values.

1) STRATEGIES NONPARAMETRIC PERFORMANCE EVALUATION

In the Wilcoxon-Mann-Whitney test, the outcomes (for all SNR levels) from the strategies serial and parallel are used to compute the rank-sum for a certain significance level in order to compare the estimation and optimization strategies. If the *p*-value is more significant than α_s, and $\mathfrak{H}_0 = 0$, the null hypothesis is accepted; otherwise, it is rejected. The hypothesis $\mathfrak{H}_0$ in these evaluations was stated as: the serial strategy results represent an improvement instead of the parallel strategy, as shown in Table 6. In addition, the samples' differences can be ranked according to the mean between them, following the Friedman and Kruskal-Wallis tests, being the lowest difference, the least similar. Table 7
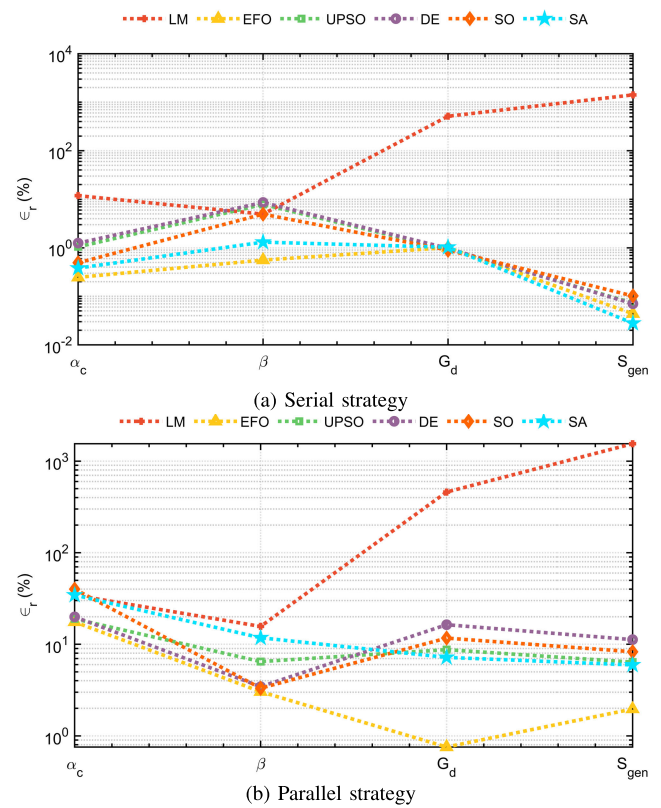
shows th results under the Friedman and Kruskal-Wallis criteria to detect the recommended strategy. Consequently, Tables 6 and 7 showed that improved estimation and optimization processes are obtained using the serial strategy compared to the parallel one, verifying the results from the statistical and parametric tests. Considering the *p*-value and $\mathfrak{H}_0$ computed from the Wilcoxon–Mann–Whitney test evaluation, the null hypothesis must is accepted. Similarly, Friedman and Kruskal-Wallis, with probability values of 0.9553 and 0.9028, respectively, ranked the serial strategy firstly.
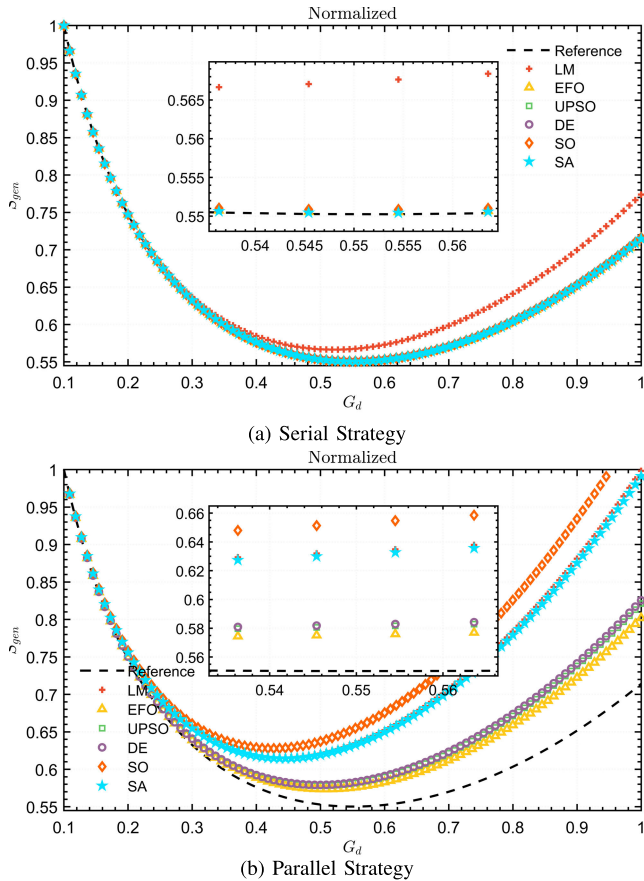
FIGURE 8. Entropy generation rate ($\dot{S}_{gen}$) profile estimation with 30 dB of AWGN by using the (a) serial and (b) parallel strategy (normalized axes).

2) RESULTS WITH LEVENBERG-MARQUARDT ALGORITHM

Being LM, a well-known optimization algorithm for solving the IHTP, it was incorporated in the previously described schemes, and its results were compared with those proposed MOAs. Fig. 7 presents the relative errors between the optimal and minimal values in the geometrical test using LM algorithm. Notice that errors using the LM were bigger than those obtained from other MOAs. For instance, the $\dot{S}_{gen}$ relative error order was around 10^3 with both strategies, serial and parallel, by using LM. Statistical results (mean (μ) and standard deviation (σ)) using the LM method in estimating $\dot{S}_{gen}$ using the serial and parallel strategies are shown in Tables 8 and 9. Numerical data shown in both last tables were far separated from the reference values given in Table 5 for all SNR levels.

B. SERIAL STRATEGY

The multiparametric strategy has been widely studied and applied in literature [4], [5]; a more profound analysis is devoted to the serial strategy. The serial strategy includes three successive tests based on geometry, build material, and working fluid (see Table 2). Besides, the estimation order was predefined, considering the parameters sensitivity of the proposed model and working on tuples as shown in Table 2. Otherwise, the relative error of the estimation process would
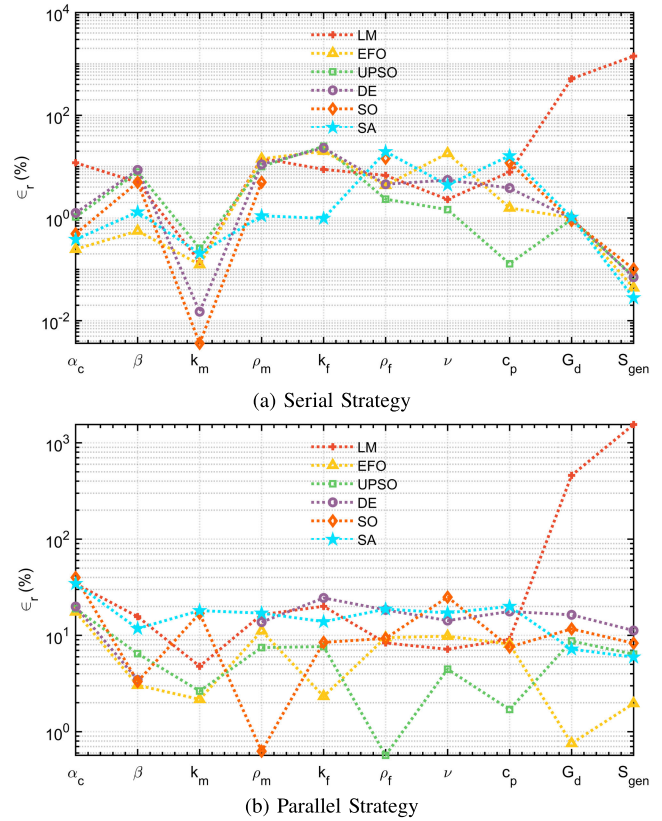

FIGURE 9. Relative errors for geometry, material, and fluid parameters using the serial and parallel strategies.

be increased. The estimation process was accomplished by reconstructing the eight estimated output parameters to feed the RMCHS mathematical model. Despite errors from each parameter estimation, the complete estimation reached less than 0.07% of relative error for 30 dB, the typical SNR of real instrumentation schemes. Similarly, despite obtaining less than 7.63% and 7.78% of relative errors in all tested MOAs using data with 10 dB and 20 dB of SNR, respectively, the results can be acceptable under specific applications, considering the strong noise influence. Moreover, considerable error propagation in the serial strategy was observed due to tests highly depending on the immediate previous results.

1) RESULTS WITH METAHEURISTICS OPTIMIZATION ALGORITHMS

The MOAs performances were also evaluated, computing the relative errors and processing times. Table 10 presents the numerical results derived from such a study. Fig. 9 shows the resulting curves from the above-described experiments. Furthermore, the accuracy performances seem similar for all MOAs with serial strategy, but considerable variations using the parallel scheme were detected. In such conditions, the processing time is a remarkable feature. EFO and DE were the fastest algorithms, according to Table 10. Likewise, DE achieved the lowest processing time for the parameter estimation process with an acceptable error per parameter

TABLE 8. Statistical results for the selected optimization algorithms for each SNR level in geometry test and serial strategy.

	SNR [dB]	α_c		β		G_d [m^3/s]		$\dot{S}_{gen}$ [W/K]	
		μ $\times 10^{-3}$	σ $\times 10^{-5}$	μ $\times 10^{0}$	σ $\times 10^{-1}$	μ $\times 10^{-3}$	σ $\times 10^{-7}$	μ $\times 10^{-1}$	σ $\times 10^{-9}$
LM	10	19.457	0.3464	1.9923	0.5707	34.600	25487	42.880	8.64×10^8
	20	**4.0947**	7.6733	**2.0745**	2.2141	38.630	51.690	69.798	2.46×10^6
	30	3.1822	5.2966	1.9759	2.0600	33.463	50804	57.395	2.13×10^9
	−	3.6016	5.9057	**2.0552**	1.9323	41.954	55381	94.212	3.21×10^9
EFO	10	9.9936	0.3486	2.2495	2.49×10^{-3}	6.7963	2.67×10^{-2}	3.4981	3.88×10^{-5}
	20	8.5420	2.4939	2.0757	0.3779	6.7024	4.51×10^{-2}	3.4920	4.63×10^{-4}
	30	**3.6035**	4.8237	**2.0906**	1.7613	5.5093	2.20×10^{-3}	3.7875	8.01×10^{-6}
	−	3.6034	4.0677	2.0494	1.6660	5.5031	2.93×10^{-2}	3.7895	3.32×10^{-4}
UPSO	10	**9.9932**	0.4592	**2.1068**	2.28×10^{-2}	6.7888	7.12×10^{-4}	3.4980	2.17×10^{-12}
	20	8.6212	3.2198	1.9307	0.1838	**6.6950**	3.05×10^{-4}	**3.4945**	5.55×10^{-8}
	30	3.6503	1.5768	1.9158	0.6917	5.5057	6.10×10^{-5}	3.7886	3.60×10^{-13}
	−	3.6421	1.6900	1.9158	0.6898	**5.4981**	1.78×10^{-4}	3.7914	1.42×10^{-15}
DE	10	10.000	9.22×10^{-19}	2.2500	9.53×10^{-25}	6.7978	8.4594	3.4980	6.1186
	20	8.6104	11.168	1.9696	1.8727	6.6992	3.9920	3.4926	2.1015
	30	3.6577	1.6853	1.8994	0.6005	5.5074	9.2044	3.7885	16.717
	−	**3.6087**	0.5965	2.0425	0.1383	5.5068	1.1077	**3.7889**	2.8214
SO	10	10.000	1.18×10^{-16}	1.8863	1.9240	**6.7758**	3.48×10^{-3}	3.4980	1.41×10^{-6}
	20	8.5193	17.217	2.0560	2.6090	6.6995	1.69×10^{-2}	3.4926	7.26×10^{-6}
	30	3.6302	0.3996	1.9759	0.1548	**5.5030**	6.10×10^{-4}	3.7885	3.55×10^{-7}
	−	3.6224	5.0118	1.9844	1.6608	5.5021	1.13×10^{-2}	**3.7889**	6.00×10^{-6}
SA	10	9.9949	0.6468	1.9305	1.1507	6.7778	5.9060	**3.4982**	1.9285
	20	8.4922	9.75×10^{-2}	2.1027	2.30×10^{-3}	6.6989	16.826	3.4932	6.6936
	30	3.5986	0.8525	2.1062	0.2983	5.5103	10.105	**3.7869**	7.9038
	−	3.6134	5.3026	2.0149	1.7873	5.5018	7.5830	3.7894	13.609

TABLE 9. Statistical results for the selected optimization algorithms for each SNR level in geometry test and parallel strategy.

	SNR [dB]	α_c		β		G_d [m^3/s]		$\dot{S}_{gen}$ [W/K]	
		μ $\times 10^{-3}$	σ $\times 10^{-4}$	μ $\times 10^{0}$	σ $\times 10^{-1}$	μ $\times 10^{-3}$	σ $\times 10^{-3}$	μ $\times 10^{-1}$	σ $\times 10^{-14}$
LM	10	15.626	33.875	**1.7898**	0.3724	46.734	1.8135	98.289	1.09×10^{14}
	20	**7.2881**	12.408	**2.0893**	1.0750	34.917	3.3496	57.858	1.50×10^{14}
	30	2.3690	2.5957	1.7530	3.31×10^{-2}	30.534	3.8333	62.444	1.82×10^{14}
	−	**3.6264**	0.5257	1.9292	1.9414	37.581	6.0000	86.046	3.48×10^{14}
EFO	10	**6.5146**	48.374	533.37	7513.1	**6.6794**	4.38×10^{-6}	4.7139	5.1028
	20	9.3939	6.8283	1.8867	1.5106	6.5966	1.43×10^{-5}	3.4907	69.586
	30	**2.9786**	8.6240	2.1421	0.8881	**5.4129**	4.80×10^{-6}	**3.8602**	13.338
	−	3.5137	1.9096	2.0430	0.1894	**5.5560**	1.56×10^{-6}	**3.7617**	2.4533
UPSO	10	9.8942	1.3695	2.0649	1.2447	7.4433	4.82×10^{-9}	3.7147	2.72×10^{-9}
	20	8.9675	6.5225	2.0441	0.3143	6.6738	2.25×10^{-8}	3.4779	1.41×10^{-8}
	30	2.9272	0.2578	1.9444	2.1824	4.9773	7.30×10^{-9}	4.0277	9.28×10^{-8}
	−	3.8386	1.9530	**2.0726**	1.0445	5.5989	2.27×10^{-8}	3.7533	3.04×10^{-9}
DE	10	10.000	2.06×10^{-17}	2.1412	1.5383	7.4737	3.35×10^{-3}	3.7189	3.55×10^6
	20	9.4144	1.9578	1.9806	0.9791	**6.5411**	3.39×10^{-3}	**3.5015**	6.30×10^6
	30	2.8923	0.8449	2.0073	1.8723	4.5617	2.10×10^{-4}	4.2114	2.26×10^5
	−	3.7704	5.6473	2.0565	0.8313	5.5974	1.27×10^{-3}	3.7397	3.01×10^5
SO	10	9.9994	7.81×10^{-3}	2.0918	2.2364	7.1323	1.16×10^{-6}	**3.7940**	9.82×10^{-2}
	20	9.6576	4.7616	2.0007	3.3868	6.7976	9.59×10^{-7}	3.4274	0.3494
	30	2.1676	3.9533	**2.0100**	3.3945	4.8168	4.32×10^{-7}	4.0997	6.68×10^{-2}
	−	2.8687	19.236	2.1898	0.8502	4.8147	8.48×10^{-7}	4.0160	1.1344
SA	10	9.9014	1.3149	1.9677	1.1448	7.3840	3.07×10^{-4}	3.6059	1.51×10^5
	20	9.5834	5.6789	1.9110	1.6189	7.0107	1.37×10^{-2}	3.4014	4.69×10^7
	30	2.3657	2.0858	1.8340	0.7135	5.0616	5.17×10^{-3}	4.0112	2.77×10^7
	−	3.3923	0.5325	2.0358	2.5531	5.6922	1.19×10^{-4}	3.7255	2.32×10^5

and, consequently, for the $\dot{S}_{gen}$ profile and minimal value result.

Further, from Table 10, EFO and DE showed to be approximatively eight and twenty times faster than LM, respectively, with minimal relative errors in the $\dot{S}_{gen}$ profile and minimal value estimation. The overall procedure estimated the RMCHS channel dimensions shown in Table 11 for the volume $L_D \times W_D \times H_D = 75\ \mu\text{m}^3$. This experiment considered

TABLE 10. Entropy generation rate ($\dot{S}_{gen}$) relative error and processing time (t) for selected optimization algorithms in geometry, material, and fluid tests, and serial strategy.

	SNR [dB]	$\dot{S}_{gen}$ [W/K]	t [s]		
		% ϵ_r	Geo	Mat	Flu
LM	10	1032.3	40.887	48.846	138.06
	20	1743.1	44.173	58.930	109.36
	30	1415.6	46.968	45.359	108.09
	–	2387.8	47.008	42.573	127.98
EFO	10	7.6287	4.7708	4.5994	4.5970
	20	7.7898	4.0039	3.8926	4.6951
	30	0.0132	3.1666	3.3451	3.6711
	–	0.0660	4.7868	5.8149	4.3240
UPSO	10	7.6314	32.231	30.803	29.568
	20	**7.7238**	36.505	33.980	36.454
	30	0.0422	33.479	33.021	29.652
	–	0.1162	38.835	35.958	34.938
DE	10	7.6314	**1.6675**	**1.5106**	**1.4964**
	20	7.7740	**2.4454**	**1.9776**	**1.8310**
	30	0.0396	**1.6324**	**1.7298**	**1.8736**
	–	**0.0502**	**1.9186**	**2.0269**	**1.5099**
SO	10	7.6314	30.759	35.616	35.069
	20	7.7898	31.223	34.259	35.247
	30	0.0713	30.292	36.367	32.601
	–	0.0739	32.128	37.804	39.885
SA	10	**7.6261**	44.544	35.992	46.145
	20	7.7581	16.906	63.165	41.685
	30	**0.0026**	19.709	40.160	28.216
	–	0.0634	24.836	81.357	19.077

TABLE 11. Optimal dimensions computed for the RMCHS design using aluminum and air working fluid.

Material	Fluid	h_c^* [mm]	w_c^* [μm]	w_p^* [μm]	N_c^*
Al	Air	25	45.125	21.759	372.

$L_D = 50$ mm, $W_D = 50$ mm, $H_D = 30$ mm, as well as the equations (1)-(4) and the optimal values in Table 5.

2) OPTIMIZATION ALGORITHMS NONPARAMETRIC PERFORMANCE EVALUATION

According to the non-free-lunch theorem [45], in a great diversity of applied problems, most optimization algorithms behave on average similarly in a great diversity of applied problems. The particular conditions of the application may strongly influence the performance of the algorithms, and consequently, selecting the most suitable algorithm. In this case, for comparing the process of estimation and optimization performances for each used algorithm, the outputs (for all SNR levels) from each algorithm, LM and MOAs (EFO, UPSO, DE, SO, and SA) are used to compute the rank-sum with a specific significance level. The $\mathfrak{H}_0$ was stated as: the results from every tested MOA express an improvement regarding the LM outcomes.

a: EVALUATION BY WILCOXON–MANN–WHITNEY TEST

According to Table 12 and regardless of the used strategy, all MOAs represent an improvement in estimating and optimizing process; there is enough evidence (*p*-values and $\mathfrak{H}_0$)

TABLE 12. Wilcoxon–Mann–Whitney test results with a significance level of $\alpha_s = 0.01$ for comparison between LM and MOAs in serial and parallel strategies.

Comparison	Strategy	*p*-value	$\mathfrak{H}_0$	Rank-sum
LM vs. EFO	Serial	**0.9202**	0	301
	Parallel	0.8950	0	**297**
LM vs. UPSO	Serial	0.9838	0	**320**
	Parallel	**0.9883**	0	323
LM vs. DE	Serial	**0.9766**	0	316
	Parallel	0.9602	0	**310**
LM vs. SO	Serial	**0.9907**	0	325
	Parallel	0.9309	0	**303**
LM vs. SA	Serial	0.9634	0	**311**
	Parallel	**0.9924**	0	327

TABLE 13. Friedman test results and ranking of algorithms with a significance level of $\alpha_s = 0.01$ for comparison between LM and MOAs in serial and parallel strategies. (Best algorithms are ranked from left to right).

Strategy	*p*-values	Statistics	Ranking					
Serial	0.2278		SO	SA	UPSO	DE	EFO	LM
		μ-rank	**5.6563**	5.7500	5.8750	6.5313	6.7188	8.4688
		σ-rank	3.5992	3.5992	3.5992	3.5992	3.5992	3.5992
Parallel	0.2697		SA	EFO	SO	UPSO	DE	LM
		μ-rank	**5.2500**	6.0000	6.250	6.500	6.687	8.312
		σ-rank	3.6055	3.6055	3.6055	3.6055	3.6055	3.6055

TABLE 14. Kruskal-Wallis test results and ranking of algorithms with a significance level of $\alpha_s = 0.01$ for comparison between LM and MOAs in serial and parallel strategies. (Best algorithms are ranked from left to right).

Strategy	*p*-values	Statistics	Ranking					
Serial	0.1474	μ-rank	SO	UPSO	DE	SA	EFO	LM
			39.656	43.250	44.344	46.625	52.781	64.344
Parallel	0.1079	μ-rank	SA	UPSO	DE	SO	EFO	LM
			37.437	41.312	44.750	51.625	52.375	63.500

to accept the null hypothesis. In serial strategy, the highest *p*-value belongs to SO with 0.9907 and a rank-sum of 325. Simultaneously, the best *p*-value (0.9924) with 327 of rank-sum occurs with SA in the parallel strategy.

b: EVALUATION BY FRIEDMAN

According to the Friedman test, Table 13 shows the ranking of algorithms (traditional and nontraditional) to estimate and optimize RMCHS model parameters. There were coincidences about the worst performance algorithm (LM) in both strategies because of obtaining the highest μ-rank. Conversely, SO and SA were the best in the serial and parallel strategies, respectively.

c: EVALUATION BY KRUSKAL-WALLIS

Table 14 presents the algorithms ranking following the Kruskal-Wallis test; there were differences between the serial and parallel strategies results in the first and fourth positions, where the SO and SA algorithms exchanged ranked positions each other precisely. Once again, the SO achieved the best

performance for serial, the same with SA for parallel one. For both the Friedman and Kruskal-Wallis tests, the smallest means were achieved by the parallel strategy.

C. CONTRIBUTIONS

The main contribution of this work is to propose reliable methodologies to overcome the practical disadvantages of the strategies using the traditional algorithms to solve the IHTPs, analyzing, in this case, the design of the RMCHSs. First, the RMCHS model is achieved through the EGM criterion instead of the classical thermodynamics laws-based modeling process. Details and advantages about using this criterion were previously studied by Cruz-Duarte *et al.* [17], [30]. Second, the serial strategy changes the optimization paradigm, improving the results considering the active influence of the model parameters, prioritizing the most influential parameters grouping them in *n*-tuples according to the case, as shown in Table 2. Once the parameters are grouped and organized, they are sequentially estimated by MOAs. Note that by estimating a single group of parameters at a time, the optimization process is accelerated, increasing the precision because the uncertainty is reduced by using fewer variables. Once a tuple is optimized, the results are propagated into the model, and the next tuple is then processed. This rule continues into a loop until fulfilling the stopping criteria. Finally, the explored MOAs helped to surmount the LM issues associated with processing nonlinear models (*e.g.,* model discontinuities, Jacobian matrix instability, proper selection of Φ, Ω coefficients, or the starting point). Once tuned, the MOAs can be seen as unsupervised optimizers. Finding optimal solutions over the search space depends highly on the exploration-exploitation rate related to the algorithm nature.

V. ANALYSIS AND DISCUSSION

This study proposed an alternate strategy for solving the IHTP in the optimal parameters estimation sense of an RMCHS design (modeled via the EGM criterion). The proposed serial strategy includes integrating nontraditional searching algorithms for solving the associated estimation and optimization problems following a sequential process based on a sensitivity analysis of the studied parameters allowing an improvement in the overall performance. According to sensitivity analysis, such a modification was efficient in terms of accuracy and processing time, *i.e.,* the proposed method required less (or similar) time than the LM method but achieving better numerical results. In this study, the entropy generation rate criterion was used on all numerical tests. The sensitivity analysis approach helped to decide the estimation-optimization order. In this study, the geometrical variables were the most influential in the process. There was no difference between choosing material and fluid variables or vice versa. The solution development was addressed to tackling the IHTP method by using MOAs, considering the problem as a black box, *i.e.,* it is not required comprehensive knowledge about the objective function and its differential or linear properties. Hence, five metaheuristics (EFO, UPSO, DE, SO, and SA)

and the LM method were assessed. The results were quantified in relative errors, which were lower than 0.07%, 7.63%, and 7.78%, with contaminated data of 30, 10, and 20 dB, respectively, using the proposed serial strategy. UPSO, DE, and SO achieved lower values than the reference one (see Fig. 6).

Numerical results showed that the parallel strategy is more sensitive to the low SNR levels than the serial strategy. Data with high dispersion (low SNR value, *e.g.,* , 10 and 20 dB) generated disproportionate results, resulting in a disadvantage of this strategy. This is a consequence of using a least-squares fitting by OLSN, expecting new proposals of solution.

It is noteworthy that the proposed scheme allowed all optimization algorithms to reach optimal solutions. Finally, the parametric statistical tests based on mean and standard deviation were shown. Moreover, three nonparametric statistical tests were implemented to formally determine the most appropriate optimization algorithm and the most recommended solution strategy. Such formal evaluation metrics included the Wilcoxon–Mann–Whitney, Friedman, and Kruskal-Wallis evaluation tests. The parametric and nonparametric tests confirmed the obtained improvement of using the serial strategy over the parallel one, as well as on using of MOAs over the LM method.

VI. CONCLUSION

This work proposed an alternate optimal parameter estimation strategy, solving an IHTP related to thermal energy management in electronic devices. These parameters dealt with an RMCHS model design to obtain the optimal characteristics such as the geometry, building materials, and working fluids. The modeling was obtained under the EGM criterion sense. Furthermore, an inverse analysis was applied to solve an IHTP using five global population-based MOAs replacing the traditional LM algorithm and two systematical strategies, *i.e.,* serial and parallel. Specifically, the serial strategy obtained more significant accuracy and higher reliability than the parallel one (commonly used) in the estimation and optimization processes. The five MOAs (*i.e.,* EFO, UPSO, DE, SO, and SA) were implemented and analyzed. Their performances and solutions were contrasted against the deterministic LM method.

To summarize, a serial scheme powered with either MOAs (depending on the computing platform capabilities and earlier sensitivity analysis) represents an excellent strategy for solving the IHTP associated with the RMCHS design in thermal energy management. Therefore, the serial strategy can be considered a thoughtful alternate for the parameter estimation when complex and highly nonlinear models are studied despite observing an accumulation of error propagation due to tests depending on previous results (sequential process). It is noticed that this approach is suitable for microelectronics applications, even for contaminated signals of 10 dB or 20 dB of SNR as measured data. The serial strategy is recommended for designing RMCHSs using the

inverse heat transfer problem, as shown in this work, formally validated by three nonparametric tests (Wilcoxon–Mann–Whitney, Friedman, and Kruskal-Wallis) during comparisons of strategies and optimization algorithms. Using MOAs in the estimation-optimization processes avoids finding the main drawbacks of the LM algorithm (instability, gradient discontinuities, or nonlinearities issues). These MOAs achieve behave as unsupervised optimizers, and proper tuning of their parameters can be increased the exploration-exploitation rate to improve all the processes.

CONFLICTS OF INTEREST
The authors declare there is no conflict of interest.

REFERENCES

[1] B. Chen, "Heterogeneous integration roadmap—A vision to the future," *IEEE Electron. Packag. Soc. Newslett.*, vol. 40, no. 1, pp. 12–13, Jan. 2018.

[2] D. B. Tuckerman and R. F. W. Pease, "High-performance heat sinking for VLSI," *IEEE Electron Device Lett.*, vol. EDL-2, no. 5, pp. 126–129, May 1981.

[3] X.-D. Wang, B. An, L. Lin, and D.-J. Lee, "Inverse geometric optimization for geometry of nanofluid-cooled microchannel heat sink," *Appl. Thermal Eng.*, vol. 55, nos. 1–2, pp. 87–94, Jun. 2013.

[4] Z.-H. Wang, X.-D. Wang, W.-M. Yan, Y.-Y. Duan, D.-J. Lee, and J.-L. Xu, "Multi-parameters optimization for microchannel heat sink using inverse problem method," *Int. J. Heat Mass Transf.*, vol. 54, nos. 13–14, pp. 2811–2819, Jun. 2011.

[5] X.-D. Wang, B. An, and J.-L. Xu, "Optimal geometric structure for nanofluid-cooled microchannel heat sink under various constraint conditions," *Energy Convers. Manage.*, vol. 65, pp. 528–538, Jan. 2013.

[6] A. A. Khan, S.-M. Kim, and K.-Y. Kim, "Multi-objective optimization of an inverse trapezoidal-shaped microchannel," *Heat Transf. Eng.*, vol. 37, no. 6, pp. 571–580, Apr. 2016.

[7] A. M. Adham, N. Mohd-Ghazali, and R. Ahmad, "Optimization of a rectangular microchannel heat sink using entropy generation minimization (EGM) and genetic algorithm (GA)," *Arabian J. Sci. Eng.*, vol. 39, no. 10, pp. 7211–7222, Oct. 2014.

[8] H. S. Lee, *Thermal Design: Heat Sinks, Thermoelectrics, Heat Pipes, Compact Heat Exchangers, Solar Cells*, 1st ed. Hoboken, NJ, USA: Wiley, 2010.

[9] M. N. Ozisik, *Inverse Heat Transfer: Fundamentals Application*, 1st ed. London, U.K.: Taylor & Francis, 2000.

[10] R. N. Prithiviraajan, S. Somasundharam, and K. S. Reddy, "Development of experimental methodology for estimation of thermo-physical properties of engineering materials using inverse method," *Thermal Sci. Eng. Prog.*, vol. 22, May 2021, Art. no. 100832.

[11] O. M. Alifanov, *Iterative Regularization Inverse Problems* (International Series in Heat and Mass Transfer). Berlin, Germany: Springer, 1994, ch. 9, pp. 227–328.

[12] J. V. Beck and K. A. Woodbury, "Inverse problems and parameter estimation: Integration of measurements and analysis," *Meas. Sci. Technol.*, vol. 9, no. 6, pp. 839–847, Jun. 1998.

[13] A. N. Tikhonov, "Inverse problems in heat conduction," *J. Eng. Phys.*, vol. 29, no. 1, pp. 816–820, 1975.

[14] C.-H. Huang and P.-C. Chiang, "An inverse study to design the optimal shape and position for delta winglet vortex generators of pin-fin heat sinks," *Int. J. Thermal Sci.*, vol. 109, pp. 374–385, Nov. 2016.

[15] C.-H. Huang and W.-L. Chang, "An inverse design method for optimizing design parameters of heat sink modules with encapsulated chip," *Appl. Thermal Eng.*, vol. 40, pp. 216–226, Jul. 2012.

[16] H. Ermagan and R. Rafee, "Geometric optimization of an enhanced microchannel heat sink with superhydrophobic walls," *Appl. Thermal Eng.*, vol. 130, pp. 384–394, Feb. 2018.

[17] J. M. Cruz-Duarte, A. Garcia-Perez, I. M. Amaya-Contreras, and C. R. Correa-Cely, "Designing a microchannel heat sink with colloidal coolants through the entropy generation minimisation criterion and global optimisation algorithms," *Appl. Thermal Eng.*, vol. 100, pp. 1052–1062, May 2016.

[18] A. Soleimani, A. Sattari, and P. Hanafizadeh, "Thermal analysis of a microchannel heat sink cooled by two-phase flow boiling of Al₂O₃ HFE-7100 nanofluid," *Thermal Sci. Eng. Prog.*, vol. 20, Dec. 2020, Art. no. 100693.

[19] H. Shen, X. Jin, F. Zhang, G. Xie, B. Sunden, and H. Yan, "Computational optimization of counter-flow double-layered microchannel heat sinks subjected to thermal resistance and pumping power," *Appl. Thermal Eng.*, vol. 121, pp. 180–189, Jul. 2017.

[20] W. Khan, M. Yovanovich, and J. Culham, "Optimization of microchannel heat sinks using entropy generation minimization method," in *Proc. Annu. Semiconductor Thermal Meas. Manage. Symp.*, May 2006, 2006, pp. 78–86.

[21] A. Bejan, *Entropy Generation Minimization: The Method of Thermodynamic Optimization of Finite-Size Systems and Finite-Time Processes*, 1st ed. Boca Raton, FL, USA: CRC Press, 1995.

[22] H. Jiang, J. Wang, J. Wu, and W. Geng, "Comparison of numerical methods and Metaheuristic optimization algorithms for estimating parameters for wind energy potential assessment in low wind regions," *Renew. Sustain. Energy Rev.*, vol. 69, pp. 1199–1217, Mar. 2017.

[23] G. Stolz, "Numerical solutions to an inverse problem of heat conduction for simple shapes," *J. Heat Transf.*, vol. 82, no. 1, p. 20, 1960.

[24] F. D. M. Neto and A. J. da Silva Neto, *An Introduction to Inverse Problems With Application*, 1st ed. Cham, Switzerland: Springer, 2012.

[25] H. Abedinpourshotorban, S. Mariyam Shamsuddin, Z. Beheshti, and D. N. A. Jawawi, "Electromagnetic field optimization: A physics-inspired Metaheuristic optimization algorithm," *Swarm Evol. Comput.*, vol. 26, pp. 8–22, Feb. 2016.

[26] K. E. Parsopoulos, "UPSO: A unified particle swarm optimization scheme," *Lect. Ser. Comput. Comput. Sci.*, vol. 1, pp. 868–873, Mar. 2004.

[27] R. Storn and K. Price, "Differential evolution–A simple and efficient heuristic for global optimization over continuous spaces," *J. Global Optim.*, vol. 11, no. 4, pp. 341–359, 1997.

[28] K. Tamura and K. Yasuda, "Spiral optimization—A new multipoint search method," in *Proc. IEEE Int. Conf. Syst., Man, Cybern.*, Oct. 2011, pp. 1759–1764.

[29] S. Kirkpatrick, C. D. Gelatt, and M. P. Vecchi, "Optimization by simulated annealing," *Science*, vol. 220, no. 4598, pp. 671–680, 1983.

[30] J. M. Cruz-Duarte, I. Amaya, J. C. Ortíz-Bayliss, and R. Correa, "Solving microelectronic thermal management problems using a generalized spiral optimization algorithm," *Int. J. Speech Technol.*, vol. 4, pp. 1–22, Jan. 2021.

[31] J. Kennedy and R. Eberhart, "Particle swarm optimization," in *Proc. ICNN*, vol. 4. Nov./Dec. 1995, pp. 1942–1948.

[32] J. Euzenat and J. Domingue, Eds., *Artificial Intelligence: Methodology, Systems, and Applications* (Lecture Notes in Computer Science), vol. 4183. Berlin, Germany: Springer, 2006,

[33] M. Tang, W. Long, H. Wu, K. Zhang, Y. A. W. Shardt, T. Shindo, J. Xiao, T. Kurihara, S. Arora, S. B. Singh, N. Singh, S. B. Singh, W. Zhi-Gang, M. Mavrovouniotis, C. Li, S. Yang, Z. N. Alqattan, and R. Abdullah, "A survey of swarm intelligence for dynamic optimization: Algorithms and applications," *Swarm Evol. Comput.*, vol. 2017, no. 4, pp. 1–14, 2017.

[34] Y. Zhang, S. Wang, G. Ji, Y. Zhang, S. Wang, and G. Ji, "A comprehensive survey on particle swarm optimization algorithm and its applications," *Math. Problems Eng.*, vol. 2015, Feb. 2015, Art. no. 931256.

[35] K. Tamura and K. Yasuda, "Spiral dynamics inspired optimization," *J. Adv. Comput. Intell. Intell. Inform.*, vol. 15, no. 8, pp. 1116–1122, 2011.

[36] K. Tamura and K. Yasuda, "Primary study of spiral dynamics inspired optimization," *IEEJ Trans. Electr. Electron. Eng.*, vol. 6, no. S1, pp. S98–S100, Feb. 2011.

[37] J. S. Dai, "Euler–rodrigues formula variations, quaternion conjugation and intrinsic connections," *Mech. Mach. Theory*, vol. 92, pp. 144–152, Oct. 2015.

[38] N. Metropolis, A. W. Rosenbluth, M. N. Rosenbluth, A. H. Teller, and E. Teller, "Equation of state calculations by fast computing machines," *J. Chem. Phys.*, vol. 21, no. 6, pp. 1087–1092, Jun. 1953.

[39] M. Jamil and X. S. Yang, "A literature survey of benchmark functions for global optimisation problems," *Int. J. Math. Model. Numer. Optim.*, vol. 4, no. 2, p. 150, 2013.

[40] A. M. Adham, N. Mohd-Ghazali, and R. Ahmad, "Optimization of an ammonia-cooled rectangular microchannel heat sink using multi-objective non-dominated sorting genetic algorithm (NSGA2)," *Heat Mass Transf.*, vol. 48, no. 10, pp. 1723–1733, Oct. 2012.

[41] K. Opara and J. Arabas, "Benchmarking procedures for continuous optimization algorithms," *J. Telecommun. Inf. Technol.*, vol. 7, pp. 73–80, Sep. 2011.

[42] J. Derrac, S. García, D. Molina, and F. Herrera, "A practical tutorial on the use of nonparametric statistical tests as a methodology for comparing evolutionary and swarm intelligence algorithms," *Swarm Evol. Comput.*, vol. 1, no. 1, pp. 3–18, Mar. 2011.

[43] S. García, D. Molina, M. Lozano, and F. Herrera, "A study on the use of non-parametric tests for analyzing the evolutionary algorithms' behaviour: A case study on the CEC'2005 special session on real parameter optimization," *J. Heuristics*, vol. 15, no. 6, pp. 617–644, Dec. 2009.

[44] J. Carrasco, S. García, M. M. Rueda, S. Das, and F. Herrera, "Recent trends in the use of statistical tests for comparing swarm and evolutionary computing algorithms: Practical guidelines and a critical review," *Swarm Evol. Comput.*, vol. 54, May 2020, Art. no. 100665.

[45] D. H. Wolpert and W. G. Macready, "No free lunch theorems for optimization," *IEEE Trans. Evol. Comput.*, vol. 1, no. 1, pp. 67–82, Apr. 1997.

JUAN GABRIEL AVINA-CERVANTES received the B.S. degree in communications and electronics engineering and the master's degree in electrical engineering (instrumentation and digital systems) from the University of Guanajuato, in 1998 and 1999, respectively, and the Ph.D. degree in informatics and telecommunications from the LAAS-CNRS, Institut National Polytechnique de Toulouse, France, in 2005. He is currently a Researcher and a full-time Professor with the University of Guanajuato. His research interests include the artificial vision for outdoor mobile robotics, pattern recognition, optimal control systems, and image processing.

DAVID MATAJIRA-RUEDA received the B.Eng. degree in electronics engineering from the Universidad Industrial de Santander, Bucaramanga, Colombia, in 2015, the M.Eng. degree in electrical engineering (instrumentation and digital systems) from the Universidad de Guanajuato, Guanajuato, Mexico, in 2017, where he is currently pursuing the Ph.D. degree in electrical engineering. His research interests include optimization algorithms, optimal design, data processing, applied mathematics, numerical methods, numerical analysis, bio-engineering, thermodynamics, and the inverse heat transfer problem.

MARIO ALBERTO IBARRA-MANZANO (Member, IEEE) received the B.Eng. degree in communication and electronic engineering and the M.Eng. degree in electric from the University of Guanajuato, Mexico, in 2003 and 2006, respectively, and the Ph.D. degree (Hons.) from the Institut National des Sciences Appliquées, Toulouse, France. He is currently an Assistant Professor with the Department of Electronics Engineering, University of Guanajuato. His research interest includes digital design on FPGA for image processing applied on autonomous robots and real-time systems.

JORGE MARIO CRUZ-DUARTE (Member, IEEE) was born in Ocaña, Colombia, in 1990. He received the B.Sc. and M.Sc. degrees in electronics engineering from the Universidad Industrial de Santander, Bucaramanga, Colombia, in 2012 and 2015, respectively, and the Ph.D. degree in electrical engineering from the Universidad de Guanajuato, Guanajuato, Mexico, in 2018.

Since 2019, he is a Postdoctoral Fellow with the Research Group with Strategic Focus in Intelligent Systems, Tecnológico de Monterrey, Monterrey, Mexico. His research interests include data science, optimization, mathematical methods, thermodynamics, digital signal processing, electronic thermal management, and fractional calculus. He is a member of the Mexican National System of Researcher.

RODRIGO CORREA received the B.E. degree in chemical engineering from the Universidad Nacional de Colombia, Bogotá, Colombia, the M.Sc. degree in chemical engineering from the Universidad Industrial de Santander, Bucaramanga, Colombia, and the M.Sc. and Ph.D. degrees in polymer science and engineering from Lehigh University, Bethlehem, PA, USA.

He is currently a full-time Professor with the School of Electrical, Electronic, and Telecommunication Engineering, Universidad Industrial de Santander. His research interests include microwave heating, global optimization, heat transfer, and polymers.

• • •